JACS
JOURNAL OF THE AMERICAN CHEMICAL SOCIETY
Communication
pubs.acs.org/JACS

In Situ Imaging of On-Surface, Solvent-Free Molecular Single-Crystal Growth

Guangfeng Liu,[†] Jie Liu,[†] Hao Sun,[§] Xiaoxin Zheng,[†] Yang Liu,*[,†] Xiaomin Li,[‡] He Qi,[‡] Xuedong Bai,[‡] Kenneth A. Jackson,[#] and Xutang Tao*[,†]

[†]State Key Laboratory of Crystal Materials, Shandong University, Jinan, Shandong 250100, P. R. China
[§]Bruker (Beijing) Scientific Technology Co., Ltd., Beijing 100081, P. R. China
[‡]Institute of Physics, Chinese Academy of Sciences, Beijing 100190, P. R. China
[#]Department of Materials Science and Engineering, The University of Arizona, Tucson, Arizona 85721, United States

Supporting Information

ABSTRACT: The formation of crystalline materials has been studied for more than a century. Recent discoveries about the self-assembly of many inorganic materials, involving aggregation of nanoparticle (NP) precursors or pre-nucleation clusters, challenge the simple assumptions of classical crystallization theory. The situation for organic materials is even more of a terra incognita due to their high complexity. Using in situ high-temperature atomic force microscopy during the solvent-free crystallization of an organic compound [Ni(quinolone-8-thiolate)$_2$], we observe long-range migration of NPs on a silica substrate and their incorporation into larger crystals, suggesting a non-classical pathway in the growth of the molecular crystal.

Crystal growth and solidification processes are basic to the preparation of many materials, from metals and semiconductor devices to pharmaceuticals.[1] The mechanisms of crystal growth are central to the science and process engineering of these materials. Studying the microscopic kinetics of crystallization is important for understanding these processes.[1b,2] Recently, crystallization from solutions of many inorganic materials has been successfully recorded using advanced high-tech microscopy techniques. Based on these investigations, non-classical pathways, such as "oriented attachment" of nanoparticles (NPs) followed by diffusion-controlled surface reconstruction, have been revealed. The picture that has emerged encompasses many materials, including nucleation of intermetallic compounds[3] and magnetic materials,[4] assembly of semiconductor/superconductor nanomaterials,[5] nucleation of calcium minerals,[6] and silicalite growth.[7] In the growth of some chiral crystals, such as $NaBrO_3$ and $NaClO_3$, an enantiomer-specific oriented attachment mechanism has been discovered during the "Viedma ripening" process.[8] These studies demonstrate alternate and often complementary pathways to the classical pathway that visualizes the initial formation of crystalline solids by spontaneous agglomeration of individual atoms, ions, or molecules.[9]

Understanding the crystallization of organic molecules has been a long-standing challenge, because unlike the stable covalent or atomic bonds in inorganic materials, the self-assemblies involved in organic crystals are more complex and unstable.[10] So far, the crystallization of molecular materials has been studied mainly by means of diffraction, spectroscopy, ex situ transmission electron microscopy (TEM), and simulations employing colloids or proteins as "artificial molecules",[9a,11] which do not really visualize the real microscopic kinetic processes. In particular, no experimental evidence has been found to prove whether the NP-mediated non-classical growth mechanism applies to the assembly of organic materials. Furthermore, although the fundamental dynamic mechanisms of solid-to-solid (s-s) crystallization have been studied extensively in simple systems such as silicon and germanium, they have rarely been investigated in detail for molecular compounds. Thus, despite their significance in micro-morphology control and property tuning of functional organic materials and pharmaceuticals, only a poor understanding has been developed for these issues.[12] On-surface crystallization studies may provide a precious opportunity to observe the details of the mass transport during the process in real time.

Here we report an in situ study of the solution-free, on-surface crystallization of a metal−organic coordination compound, [Ni(quinolone-8-thiolate)$_2$] ([Ni(qt)$_2$]), where polycrystalline films convert into single crystals during thermal annealing. Real-time imaging of the dynamic formation of the crystals using atomic force microscopy (AFM) and optical microscopy (OM) reveals that particles having diameters of hundreds of nanometers are able to migrate several micrometers on a surface. The experimentally revealed NP-mediated migration and oriented attachment pathways represent a non-classical solid-state growth mechanism for molecular crystals.

Thin films of [Ni(qt)$_2$] were deposited on silicon dioxide substrates (for AFM and OM) and on lacey carbon films (for TEM observation) by vacuum vapor deposition (see Supporting Information for details). The films show identical X-ray diffraction (XRD) patterns on all substrates (Figure S1), but with peak positions different from those of the bulk crystals. This indicates that the films belong to a different crystalline phase, consistent with a previous report.[13] Crystallization of films (~50 nm thick) composed of discontinuous NPs was driven by heating on a hot-stage microscope. A remarkable growth process at 150 °C was recorded by time-resolved optical microscope images and

Received: March 12, 2015
Published: April 7, 2015

DOI: 10.1021/jacs.5b02637
J. Am. Chem. Soc. 2015, 137, 4972−4975

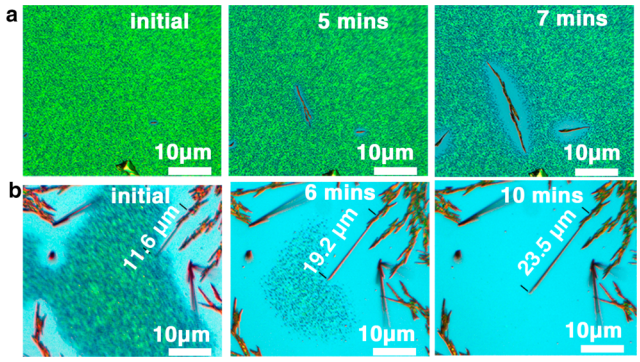

Figure 1. Optical microscopy observation of the formation of $[Ni(qt)_2]$ crystals in 50 nm thick films of $[Ni(qt)_2]$ on SiO_2 substrates. Annealing temperature, 150 °C. (a) Frames from Movie S1 show the growth of $[Ni(qt)_2]$ crystals. (b) Frames from Movie S2 show that growth of a $[Ni(qt)_2]$ single crystal is accompanied by a gradual disappearance of particles on the substrate.

is shown in Figure 1. The deposited film coarsened during heating, and then fiber-like crystals nucleated. The substrate around the larger crystals became exposed as the neighboring particles re-deposited on the larger crystals (Figure 1a and Movie S1). Another noteworthy phenomenon in the crystal formation process is shown in Figure 1b. During the growth, the single crystal behaved like a straw: the particles surrounding it on the film were absorbed into the crystal at its end, and the crystal lengthened from 11.6 to 23.5 μm (Movie S2). This suggests that NP migration is involved in the process. The typical AFM morphology of a microcrystal is shown in Figure S2, where a long and pointed "tail" grew in the film, consistent with the appearance in the optical microscope.

Our OM observations indicated that the on-surface crystallization of $[Ni(qt)_2]$ takes place by an unprecedented mode of crystal growth for molecular materials. To probe the process and obtain more structural details and dynamic information on the s-s conversion, we next used TEM. TEM imaging of pristine $[Ni(qt)_2]$ thin films (thickness ≈ 30 nm, Figure S3) displays poor continuity, with faceted NPs of ~100 nm in diameter randomly covering the lacey carbon films. After the film was heated in the TEM chamber for 10 min at 120 °C and 10^{-5} Pa, fiber-like crystals formed across the grids, as shown in Figure 2a. Simultaneously, some of the original particles near these crystals disappeared (green rectangles), similar to what was observed with OM. Figure 2a presents the selected area electron diffraction (SAED) pattern of the fiber-like crystal, showing that the top face

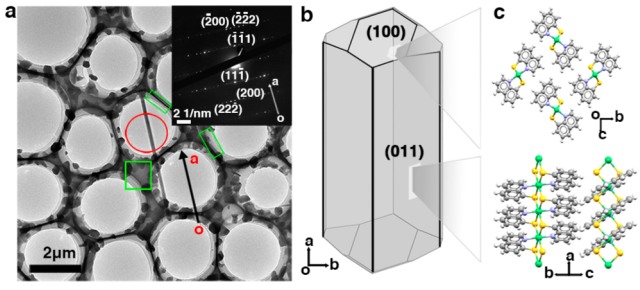

Figure 2. Formation of $[Ni(qt)_2]$ microcrystals by direct heating in the TEM chamber (120 °C and 10^{-5} Pa). (a) TEM image of a $[Ni(qt)_2]$ microcrystal; (inset) SAED patterns corresponding to the area marked with a red circle. (b) Predicted crystal morphology based on the BFDH method. (c) Crystal packing patterns of the (100) and (011) planes.

of the crystal is the (011) plane and the longitudinal direction is [100], consistent with the crystal morphology predicted by the Bravais–Friedel–Donnay–Harker (BFDH) method (Figure 2b) and the XRD results (Table S1). In the crystal structure, $[Ni(qt)_2]$ molecular layers are stacked perpendicular to the crystal growth direction, forming a one-dimensional chain structure through intermolecular S–Ni bonds along the [100] direction, as shown in the packing motifs of (100) and (011) planes in Figure 2c. Additionally, the time-related TEM results shown in Figure S4 demonstrate the formation of single crystals from the NPs. However, because of the poor stability of organic materials under the strong radiation of an electron beam (Figure S5), it is impossible to trace the transformation process of the rearrangement of the NPs in situ by using TEM.

To avoid destroying the organic materials by electron beam radiation, researchers have used AFM to observe the morphology of many organic compound films.[14] We used a Dimension Icon atomic force microscope (Bruker, Santa Barbara, CA), equipped with a heater plug (working range from ambient temperature to 250 °C) for in situ imaging of the crystallization of $[Ni(qt)_2]$ during heating. Images were collected using the ScanAsyst mode with 1.0 Hz scan rate. This mode is based on peak force tapping, which performs a very fast force curve at every pixel in the image by modulating the Z piezo at ~2 kHz with an amplitude of 150 nm. The peak force of each of these curves is then used as the imaging feedback signal. This mode controls the tip/sample interaction directly to decrease the deformation depths and the consequential contact area, so there is minimal damage to the probe or sample and higher resolution is possible. This is vital for imaging soft organic materials during heating. Commercial silicon nitride probes (ScanAsyst-Air, Bruker; spring constant ≈ 0.4 N/m) and a Stargate scanner (max. scan size ≈ 100 μm) were used to scan the sample. The samples and tips were heated at the same time to keep the same temperature by a Bruker TAC controller to avoid cantilever bending due to thermal disequilibrium.

As shown in Figure 3, the $[Ni(qt)_2]$ films were composed of many distinguishable particles on the surface, with a size of several hundred nanometers, similar to the morphology profile, as revealed by the optical and electron microscopes. Figure 3 shows sequential images depicting distinct migration trajectories of $[Ni(qt)_2]$ NPs during heating of the films at 130 °C (see Movie S3). The direct movement of a NP—such as the one marked with a yellow arrow, which constantly shifted its position from one location to another on the substrate while its shape also modified gradually—was just like a worm wriggling on the ground. In 70 min, the NP drifted ~1.6 μm, ending up between two other particles; the other surrounding NPs basically maintained their locations and shapes during this time. Another change captured in the AFM images is highlighted by the dashed line circles, where three NPs left their original positions and migrated to other positions, leaving behind an empty space. The trajectory of this migration, which seems a little fuzzier, actually corresponds to the activity of these NPs. These observations indicate the long-range migration of NPs on the SiO_2 substrate before crystallization. Ostwald ripening by the migration of adsorbed molecules, via diffusion across the surface with sequential random and short-range (~5 Å) hopping, is a well-known phenomenon in surface science.[15] Here the long-range migration of NPs cannot be explained by molecular diffusion because the NPs move as a whole and basically maintain their original shape rather than gradually disintegrating.

DOI: 10.1021/jacs.5b02637
J. Am. Chem. Soc. 2015, 137, 4972–4975

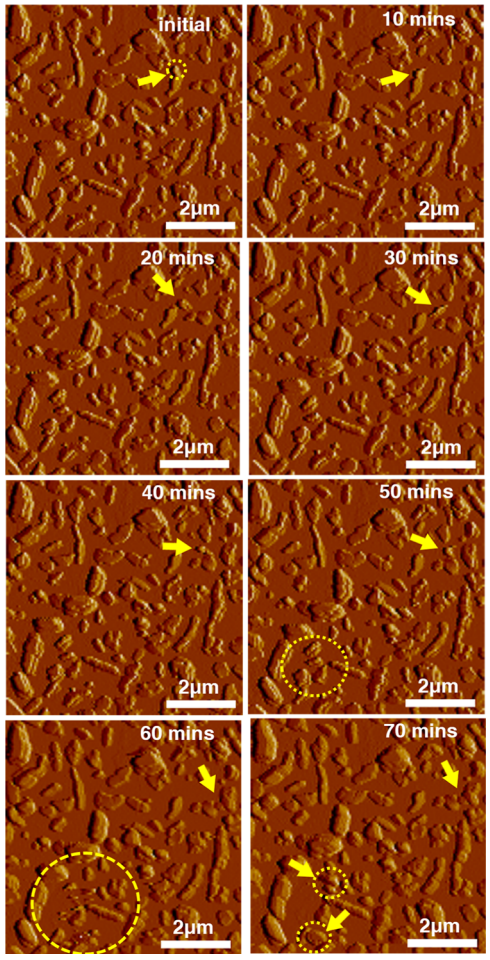

Figure 3. AFM peak force error images from Movie S3 show the migration of $[Ni(qt)_2]$ NPs before crystallization. The trajectory of NPs' migration is indicated by yellow arrows, and the remarkable changed regions on the film are highlighted by dashed circles. Film thickness, ~30 nm; annealing temperature, 130 °C.

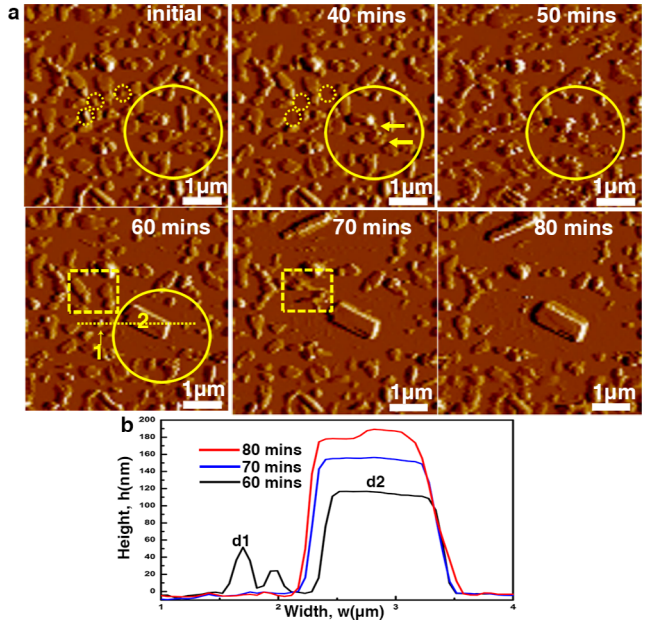

Figure 4. (a) AFM peak force error images from Movie S4 show a typical spatial−temporal evolution of the formation of a microcrystal. (b) Height profiles of line $l_{1\text{-}2}$ at various time intervals demonstrate crystal growth and surface extension. The yellow arrows, dashed and solid circles, and rectangles indicate different regions of remarkable changes on the film. Film thickness, ~30 nm; annealing temperature, 130 °C.

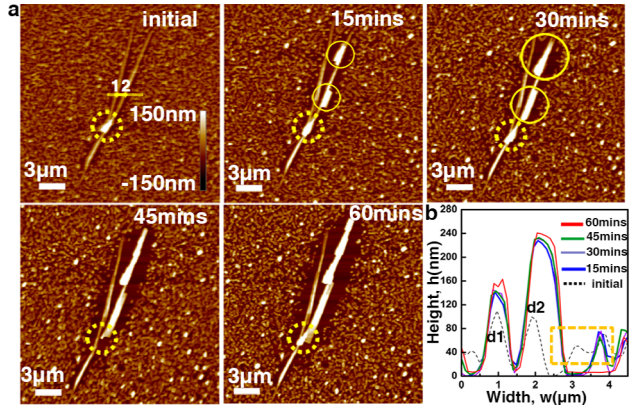

Figure 5. (a) Topographic AFM images show the evolution of the shape and dimensions of the crystals, indicating a crystal growth mechanism involving migration and re-oriented attachment of NPs to the crystal as well as Ostwald ripening. (b) Height profiles of line l_{1-2} at various times demonstrate crystal growth and surface extension. The dashed and solid circles indicate different regions of remarkable changes on the film. Film thickness, ~50 nm; annealing temperature, 130 °C.

The AFM images in Figure 4a record a stage in the formation of a $[Ni(qt)_2]$ microcrystal, demonstrating the attachment and coalescence of NPs to form microcrystals (see Movie S4). During this stage, some NPs move from their original positions and emerge in the new positions (dashed-line circles and yellow arrows). Subsequently, nearby NPs connect with each other to form irregular agglomerates (50 min). The image at 50 min is a little blurry due to the movement of the NPs during scanning, suggesting high activity of these NPs. In the image at 60 min, several NPs have fused together to form a rod crystal. After that, some other NPs near this crystal (yellow squares) move and adjust their orientation in order to attach to the crystal. The height and length of the crystal at various times are shown in Figure 4b, revealing that the nearby NPs (such as the one marked with d_1) have been absorbed by the crystal.

NP migration during the crystal growth stage may bring some abrupt expansions of the crystal on both spatial and temporal scales. As shown in Figure 5, two needle microcrystals of $[Ni(qt)_2]$ formed on heating of a 50 nm thick film at 130 °C for 1 h (initial image). After another 15 min, two additional clusters emerged and attached to the crystal along the growth direction [100], leading to remarkable increases in height in those areas (marked with two solid line circles). Continued growth of the two clusters enlarged the crystalline part along the needle, finally joining them together to make a crystal displaying a "bamboo-like" morphology (60 min). According to Figure S6 and Figure 2a, the needle crystals belong to the bulk phase of $[Ni(qt)_2]$. A noteworthy variation occurred during this process at the junction of the two needle crystals (marked with dash line circles), where a cluster detached from the crystal (45 min image), and after 15 min another cluster reattached to this position (60 min image), suggesting high activity of the clusters at this stage. To track the crystal growth concretely, we inspected the height changes by scanning across the two needle crystals along a line $l_{1\text{-}2}$. The heights of the corresponding peaks, labeled as d_1 and d_2 in Figure 5b, show a progressive increase with time, with d_2 increasing much more than d_1 due to the attachment of the two clusters on

DOI: 10.1021/jacs.5b02637
J. Am. Chem. Soc. 2015, 137, 4972−4975

the right crystal. Accompanied by crystal growth in all three dimensions, some of the surrounding NPs vanished, and the substrate became exposed around the crystals, consistent with the OM results. The scale of the exposed substrate broadened from ~100 nm to >1 μm as time elapsed (marked with dashed-line rectangle in Figure 5b). These distances are far too great to be explained by mass transport by molecular diffusion in such a solvent-free system.[16] However, direct NP migration can explain the transport of material across the gap in NPs to the crystal. After migration and attachment of the NPs to the crystal, the length and width of the crystal increased, and finally the gaps between adjacent clusters were filled. We believe this process occurs by the conventional mechanism of dissolution and growth of monomer molecules. Thus, the crystal growth mechanism involves both oriented attachment of the activated NPs and Ostwald ripening.

To validate whether a vapor transport mechanism is involved in this crystallization process, the thermal properties of $[Ni(qt)_2]$ were investigated by thermogravimetric analysis (TGA) and differential scanning calorimetry (DSC). The TG curve in Figure S7a shows a small weight loss of ~0.56% below 150 °C, which may be caused by the desorption of moisture or other solvents. The DSC curve shows a drastic endothermic peak at 359 °C due to melting. Long time measurements were carried out at 190 °C in the TGA and DSC equipment. The results are shown in Figure S7b and indicate no weight loss or heat flow variation for 4 h, excluding the possibility of sublimation of $[Ni(qt)_2]$ during crystallization. Thus, instead of vapor-phase deposition, the NPs' migration is believed to play a major role in the mass transport of this on-surface crystallization, as confirmed by the AFM observations.

We have observed a remarkable on-surface, solution-free crystal growth process of $[Ni(qt)_2]$, transforming from a polycrystalline film to single crystals, using OM, TEM, and AFM. Trajectories of NP migration were observed in the time-related AFM images, demonstrating the activity of the NPs on the surface during the crystallization process. Although the exact microstructure of the NPs and the molecular-level events governing their structural rearrangement have not yet been resolved in detail, the dynamic process of $[Ni(qt)_2]$ crystal growth identified by in situ AFM reveals a non-classical pathway in the solution-free crystallization involving NP-mediated migration and oriented attachment. We believe the results presented here offer an excellent model for understanding the crystallization of solid-state organic materials, and that understanding these mechanisms will pave the way to the rational design/preparation of molecular micro-/nanocrystalline materials with controlled properties.

■ ASSOCIATED CONTENT

Supporting Information

Experimental details, Figures S1−S7, Table S1, CIF file, and Movies S1−S4. This material is available free of charge via the Internet at http://pubs.acs.org.

■ AUTHOR INFORMATION

Corresponding Authors

*liuyangicm@sdu.edu.cn
*txt@sdu.edu.cn

Notes

The authors declare no competing financial interest.

■ ACKNOWLEDGMENTS

We thank the National Natural Science Foundation of China (grant nos. 51321091, 51227002, 51303095, and 51272129) and the Program of Introducing Talents of Disciplines to Universities in China (111 program no. b06015).

■ REFERENCES

(1) (a) Chalmers, B. *Principles of Solidification*; John Wiley & Sons: New York, 1964. (b) Jackson, K. A. *Kinetic Processes*; Wiley-VCH: Weinheim, 2010. (c) Porter, D. A.; Easterling, K. E.; Sherif, M. Y. *Phase Transformations in Metals and Alloys*; CRC Press: Boca Raton, FL, 2008. (d) Desiraju, G. R. *J. Am. Chem. Soc.* **2013**, *135*, 9952. (e) Davey, R. J.; Schroeder, S. L.; ter Horst, J. H. *Angew. Chem., Int. Ed.* **2013**, *52*, 2166. (f) Baird, J. A.; Eerdenbrugh, B. V.; Taylor, L. S. *J. Pharm. Sci.* **2010**, *99*, 3787. (g) Trasi, N. S.; Baird, J. A.; Kestur, U. S.; Taylor, L. S. *J. Phys. Chem. B* **2014**, *118*, 9974.

(2) (a) Jacobson, L. C.; Hujo, W.; Molinero, V. *J. Am. Chem. Soc.* **2010**, *132*, 11806. (b) Rimer, J. D.; An, Z.; Zhu, Z.; Lee, M. H.; Goldfarb, D. S.; Wesson, J. A.; Ward, M. D. *Science* **2010**, *330*, 337. (c) Jiang, S.; ter Horst, J. H. *Cryst. Growth Des.* **2011**, *11*, 256. (d) Vekilov, P. G. *Cryst. Growth Des.* **2010**, *10*, 5007.

(3) Liao, H.-G.; Cui, L.; Whitelam, S.; Zheng, H. R. *Science* **2012**, *336*, 1011.

(4) Li, D.; Nielsen, M. H.; Lee, J. R.; Frandsen, C.; Banfield, J. F.; De Yoreo, J. J. *Science* **2012**, *336*, 1014.

(5) (a) Cho, K.-S.; Talapin, D. V.; Gaschler, W.; Murray, C. B. *J. Am. Chem. Soc.* **2005**, *127*, 7140. (b) Boston, R.; Schnepp, Z.; Nemoto, Y.; Sakka, Y.; Hall, S. R. *Science* **2014**, *344*, 623. (c) Pacholski, C.; Kornowski, A.; Weller, H. *Angew. Chem., Int. Ed.* **2002**, *41*, 1188. (d) Tang, Z.; Kotov, N. A.; Giersig, M. *Science* **2002**, *297*, 237.

(6) (a) Van Driessche, A. E.; Benning, L. G.; Rodriguez-Blanco, J. D.; Ossorio, M.; Bots, P.; Garcia-Ruiz, J. M. *Science* **2012**, *336*, 69. (b) Pouget, E. M.; Bomans, P. H. H.; Goos, J. A. C. M.; Frederik, P. M.; de With, G.; Sommerdijk, N. A. J. M. *Science* **2009**, *323*, 1455. (c) Nielsen, M. H.; Aloni, S.; De Yoreo, J. J. *Science* **2014**, *345*, 1158.

(7) Lupulescu, A. I.; Rimer, J. D. *Science* **2014**, *344*, 729.

(8) (a) Viedma, C.; McBride, J. M.; Kahr, B.; Cintas, P. *Angew. Chem., Int. Ed.* **2013**, *52*, 10545. (b) Viedma, C. *Phys. Rev. Lett.* **2005**, *94*, 065504.

(9) (a) Sleutel, M.; Lutsko, J.; Van Driessche, A. E.; Duran-Olivencia, M. A.; Maes, D. *Nat. Commun.* **2014**, *5*, 5598. (b) Chung, S.-Y.; Kim, Y.-M.; Kim, J.-G.; Kim, Y.-J. *Nat. Phys.* **2009**, *5*, 68.

(10) (a) Harano, K.; Homma, T.; Niimi, Y.; Koshino, M.; Suenaga, K.; Leibler, L.; Nakamura, E. *Nat. Mater.* **2012**, *11*, 877. (b) Korevaar, P. A.; George, S. J.; Markvoort, A. J.; Smulders, M. M.; Hilbers, P. A.; Schenning, A. P.; De Greef, T. F.; Meijer, E. W. *Nature* **2012**, *481*, 492.

(11) (a) Yau, S. T.; Vekilov, P. G. *J. Am. Chem. Soc.* **2001**, *123*, 1080. (b) Pienack, N.; Bensch, W. *Angew. Chem., Int. Ed.* **2011**, *50*, 2014. (c) Tidhar, Y.; Weissman, H.; Tworowski, D.; Rybtchinski, B. *Chem.—Eur. J.* **2014**, *20*, 10332.

(12) (a) Boterashvili, M.; Lahav, M.; Shankar, S.; Facchetti, A.; van der Boom, M. E. *J. Am. Chem. Soc.* **2014**, *136*, 11926. (b) Park, S.-W.; Choi, J.-M.; Lee, K. H.; Yeom, H. W.; Im, S.; Lee, Y. K. *J. Phys. Chem. B* **2010**, *114*, 5661. (c) Chandaluri, Ch. G.; Radhakrishnan, T. P. *Angew. Chem., Int. Ed.* **2012**, *51*, 11849. (d) Varughese, S.; Kiran, M. S. R. N.; Solanko, K. A.; Bond, A. D.; Ramamurty, U.; Desiraju, G. R. *Chem. Sci.* **2011**, *2*, 2236. (e) Percec, V.; Holerca, M. N.; Magonov, S. N.; Yeardley, D. J. P.; Ungar, G.; Duan, H.; Hudson, S. D. *Biomacromolecules* **2001**, *2*, 706.

(13) Pilia, L.; Serri, M.; Matsushita, M. M.; Awaga, K.; Heutz, S.; Robertson, N. *Adv. Funct. Mater.* **2014**, *24*, 2383.

(14) Coltonet, R. J.; et al. *Procedures in Scanning Probe Microscopies*; J. Wiley & Sons: New York, 1998.

(15) Briner, B. G.; Doering, M.; Rust, H.-P.; Bradshaw, A. M. *Science* **1997**, *278*, 257.

(16) (a) Harikumar, K. R.; Polanyi, J. C.; Zabet-Khosousi, A.; Czekala, P.; Lin, H.; Hofer, W. A. *Nat. Chem.* **2011**, *3*, 400. (b) Komeda, T.; Kim, Y.; Kawai, M.; Persson, B. N. J.; Ueba, H. *Science* **2002**, *295*, 2055.

DOI: 10.1021/jacs.5b02637
J. Am. Chem. Soc. 2015, 137, 4972−4975